Asian Journal of Pharmaceutical Sciences 19 (2024) 100953

Available online at www.sciencedirect.com

ScienceDirect

journal homepage: www.elsevier.com/locate/AJPS

Research Article

Electrostatic spraying for fine-tuning particle dimensions to enhance oral bioavailability of poorly water-soluble drugs

Jung Suk Kim[a,1], *Seunghyun Cheon*[a,1], *Mi Ran Woo*[a], *Sanghyun Woo*[a], *Jee-Eun Chung*[a], *Yu Seok Youn*[b], *Kyung Taek Oh*[c], *Soo-Jeong Lim*[d], *Sae Kwang Ku*[e], *Bao Loc Nguyen*[f], *Jong Oh Kim*[f,*], *Sung Giu Jin*[g,*], *Han-Gon Choi*[a,*]

[a] *College of Pharmacy, Hanyang University, Ansan 15588, South Korea*
[b] *School of Pharmacy, Sungkyunkwan University, Suwon 440746, South Korea*
[c] *College of Pharmacy, Chung-Ang University, Seoul 156-756, South Korea*
[d] *Department of Bioscience and biotechnology, Sejong University, Seoul 143747, South Korea*
[e] *Department of Anatomy and Histology, College of Korean Medicine, Daegu Haany University, Gyeongsan 38610, South Korea*
[f] *College of Pharmacy, Yeungnam University, Gyongsan 712749, South Korea*
[g] *Department of Pharmaceutical Engineering, Dankook University, Cheonan 31116, South Korea*

ARTICLE INFO

Article history:
Received 23 April 2024
Revised 6 June 2024
Accepted 14 June 2024
Available online 22 August 2024

Keywords:
Electrostatic spray drying
Poorly water-soluble drug
Regorafenib
Particle size distribution
Oral bioavailability
Oral antitumor efficacy

ABSTRACT

While spray-drying has been widely utilized to improve the bioavailability of poorly water-soluble drugs, the outcomes often exhibit suboptimal particle size distribution and large particle sizes, limiting their effectiveness. In this study, we introduce electrostatic spraying as an advanced technology tailored for poorly water-soluble drugs, enabling the fabrication of nanoparticles with fine and uniform particle size distribution. Regorafenib (1 g), as a model drug, copovidone (5 g), and sodium dodecyl sulfate (0.1 g) were dissolved in 200 ml ethanol and subjected to conventional-spray-dryer and electrostatic spray dryer. The electrostatic spray-dried nanoparticles (ESDN) showed smaller particle sizes with better uniformity compared to conventional spray-dried nanoparticles (CSDN). ESDN demonstrated significantly enhanced solubility and rapid release in water. *In vitro* studies revealed that ESDN induced apoptosis in HCT-116 cells to a greater extent, exhibiting superior cytotoxicity compared to CSDN. Furthermore, ESDN substantially improved oral bioavailability and antitumor efficacy compared to CSDN. These findings suggest that ESD shows potential in developing enhanced drug delivery systems for poorly water-soluble drugs, effectively addressing the limitations associated with CSD methods.

* Corresponding authors.
E-mail addresses: jongohkim@yu.ac.kr (J.O. Kim), sklover777@dankook.ac.kr (S.G. Jin), hangon@hanyang.ac.kr (H.-G. Choi).
[1] These authors contributed equally to this work.
Peer review under responsibility of Shenyang Pharmaceutical University.

https://doi.org/10.1016/j.ajps.2024.100953

1. Introduction

Nano-drug delivery systems have become a cornerstone in pharmaceutical research, offering significant advancements in enhancing the oral bioavailability of poorly water-soluble drugs [1-4]. Leveraging their nano-scale dimensions, these systems provide a multitude of advantages, such as preventing premature degradation of the drug, improving intracellular penetration, and increasing drug absorption [5-8]. Conventional spray-drying (CSD) has been a prominent technique for nanoparticle preparation due to its rapid solvent evaporation capability and scalability [9,10]. Its widespread adoption in the pharmaceutical industry is attributed to its capacity for high-yield mass production of particles [11]. However, spray drying generally produces relatively large and irregular particles, which reduce the advantages of nano-scale unit.

Electrospinning and electrospraying have emerged as advanced alternatives to spray drying for the production of fine nanoparticles. These technologies transform drug-loaded organic solution droplets into nanofibers or nanoparticles through the application of an electrical field [12,13]. Yet, despite their potential, electrospinning and electrospraying are hindered by time-consuming processes and low productivity with poor product yield, as compared to spray drying. These limitations impede large-scale applications and complicate the process of scaling up [14]. The experimenter often needs to continuously monitor "needle clogging" during the operation of these technologies, as it impacts the homogeneity of the final product [15]. Owing to these constraints, there is limited active implementation of electrospinning and electrospraying technologies within the pharmaceutical industry. Hence, the investigation into new technology for manufacturing nanoparticles would be of great value to the pharmaceutical industry.

Electrostatic spray drying (ESD) is a newly developed convergence technology characterized by its simple operating process. This innovative method incorporates a distinctive atomization mechanism that synergistically harnesses electrostatic forces alongside compressed air gas. This hybrid atomizing approach offers several notable advantages. During the ESD process, electrostatic forces facilitate the migration of solvent molecules to the outer surface while directing drugs towards the core of the droplet, effectively maximizing nano-sizing efficacy [16]. Subsequently, the application of compressed air efficiently removes the solvent from the droplets, leading to a high production rate and satisfactory yield. Additionally, the high pressure of the compressed air mitigates the risk of needle clogging, thereby reducing the need for continuous monitoring by the experimenter. Therefore, this novel technology offers significant improvements in process simplicity, productivity and particle homogeneity compared to electrospinning and electrospraying. These advantages make it particularly suitable for the pharmaceutical industry, where such characteristics contribute to improved scalability and product quality. Moreover, the transfer of solvent to the droplet's shell via electrostatic forces facilitates solvent evaporation, even at moderate drying temperatures. This feature allows for higher encapsulation efficiency, particularly beneficial for highly volatile drugs, and reduces the risk of heat-induced degradation in drugs with low melting points.

In this study, we sought to produce ESD nanoparticles (ESDN) to improve oral bioavailability of a poorly water-soluble drug. Regorafenib, commonly prescribed for colorectal carcinoma, was selected as a model drug, since its poor water-solubility limit anticancer efficacy [17,18]. The superiority of ESD was investigated through a comparison with CSD nanoparticles (CSDN) throughout the study. Physicochemical properties, aqueous solubility, oral bioavailability and anticancer efficacy of prepared systems were evaluated. Thereby, it was confirmed that the convergence of electrostatic force and spray-drying has the potential to enhance oral bioavailability of poorly water-soluble drugs.

2. Materials and methods

2.1. Materials

The drug (regorafenib anhydrous) was obtained from Boryung Pharmaceutical Co. (Ansan, South Korea). Copovidone, poloxamer 407, and polyvinylpyrrolidone were purchased from BASF (Ludwigshafen, Germany). Sodium dodecyl sulfate (SDS) and HP-β-CD were donated by Hanmi Pharm. Co. (Suwon, South Korea). Plurol diisostearique, Labrafil M1944CS, and Labrasol were bought from Gattefossé (Saint-Priest, France). Hypromellose and polyvinyl alcohol were obtained from Shin-Etsu Co. (Tokyo, Japan). Sorbitan monooleate 80 and polysorbate 80 were purchased from Daejung Chem. Co., Ltd., Siheung, South Korea). All other solvents and chemical substances were of reagent grade and used without further purification.

2.2. Effects of carrier on the solubility of regorafenib

The successful enhancement of bioavailability for poorly water-soluble drugs hinges on the careful selection of suitable carriers. Therefore, various solubilizing carriers were examined based on the established screening technique [19,20]. Briefly, drug solubility was investigated in several types of aqueous solutions containing surfactants (10 %, w/v). After selecting the surfactant with the highest drug solubility, an excess amount of regorafenib was added to 1 ml aqueous solution containing various polymers (1 %, w/v) and the selected surfactant (0.1 %, w/v). Subsequently, the polymer that increased the drug solubility the most was selected. In this study, quantitative analysis of regorafenib was performed by high-performance liquid chromatography (HPLC) (Method 1 in supplementary materials).

2.3. Manufacture of nanoparticles

In this study, two types of nanoparticles were prepared by CSD and ESD. Both comprised the drug, copovidone and SDS, according to a carrier selection study. Pure ethanol was used equally as a solvent since both systems were solvent-based.

2.3.1. CSD

The drug (1 g), copovidone (5 g) and SDS (0.1 g) were completely dissolved in 200 ml ethanol to prepare the feed solution. Subsequently, the solution was injected into a spray dryer (B-290; Büchi Co., Flawil, Switzerland) at a speed of 4.0 ml/min. As soon as the feed solution moved to the two-fluid nozzle inside the spray dryer, the solution was dispersed into fine droplets via compressed air gas. The spraying nozzle consisted of a tip with a 0.7 mm diameter hole and a nozzle cap. During the spray-drying process, the air pressure was fixed at 4 kg/cm^2, and the aspirator figure was 100%. The inlet temperature was maintained at 90 °C.

2.3.2. ESD

ESD was carried out using a Fluid Air electrostatic spray dryer system (PolarDry 0.1; Naperville, IL, USA). The feed solution was introduced to the dryer at a speed of 4.0 ml/min. The system consists of a spray chamber, collection transition, product collection sock, and a drying gas conditioning system. Electrostatic interactions occur in the spray chamber. The feed solution was pumped through an electrostatic nozzle and heated. Simultaneously, high-pressure gas and electrostatic forces atomize the feed solution. The final particles are deposited into the product collection sock, while the mixed saturated atomizing gas and drying gas pass through the filter sock to exhaust. The ESD parameters were optimized as follows: drying gas flow of 4.5 Nm^3/h, voltage fixed at 20 kV. The chamber vacuum and atomizing gas press were set to 0.5 kPA and 50 kPA, respectively. The inlet temperature was maintained at 40 °C.

2.4. Physicochemical properties

2.4.1. Laser diffraction-based size class distribution analysis

Laser diffraction-mediated analysis was carried out using a Mastersizer 3000 (Malvern, Worcestershire, UK). The air pressure was 1.0 bar and the feed rate was 50%. The size classes were expressed as D10, D50 and D90, indicating that 10%, 50% and 90% of the particles had diameters smaller than these values, respectively. Along with the particle size distribution, ESD and CSD were compared in terms of specific surface area and uniformity index.

2.4.2. Scanning electron microscope (SEM)

The dried-powder morphology was confirmed using SEM (S-4800; Hitachi, Tokyo, Japan). Before evaluation, each sample was attached to a brass disk with double-sided sticky carbon tape. Then, the samples were made electrically conductive with platinum coating using an EMI Tech Ion Sputter K575 (Quorum Technologies, Lewes, UK).

2.4.3. Differential scanning calorimetry (DSC)

Thermal analysis was conducted using a DSC Q20 (TA Instruments, New Castle, DE, USA). Each sample was placed in an aluminium pan, and the pan was sealed with an aluminium lid. Nitrogen gas flowed at a rate of 20 ml/min, and the operating temperature was constantly increased from 50 °C to 300 °C at a rate of 10 °C/min.

2.4.4. X-ray diffraction (XRD)

XRD was performed to assess the crystallinity of the samples. The instrument used for the examination was a D/MAX-2500 PC (Rigaku Co., Tokyo, Japan). The analysis conditions were as follows: scanning 2θ range from 3° to 50° with an angular increment of 0.02°/s, Cu-Kα radiation at a voltage of 40 kV, and a scan speed of 10°/min.

2.4.5. Fourier transform infrared (FTIR) spectroscopy

The FTIR spectra (4000–450 cm^{-1}) were evaluated using Frontier (PerkinElmer, Waltham, MA, USA). The utilised measurement range and resolution was 2000–800 cm^{-1} and 4 cm^{-1}, respectively.

2.4.6. Proton nuclear magnetic resonance spectrometry (^{1}H NMR) spectroscopy

^{1}H NMR experiments were performed on a Bruker Analytik ADVANCE digital 500 (Billerica, MA, USA). ^{1}H NMR spectra were generated by assessing samples dissolved in d_6-DMSO.

2.4.7. Encapsulation efficiency

The amount of the drug entrapped within the nanoparticles was analysed using the HPLC method described above. Samples of free drug powder, CSDN and ESDN, each containing an equivalent of 20 mg of the drug, were dissolved in 100 ml acetonitrile. The encapsulation efficiency was then calculated using following equation:

$$\text{Encapsulation efficiency (\%)} = (W_d/W_t) \times 100\%$$

where W_t refers theoretical drug amount and W_d refers quantified drug amount.

2.4.8. Dynamic light scattering-based particle size analysis

After dissolving the nanoparticles in water, the particle size was evaluated using a Zetasizer Nano ZS (Malvern Instruments, Worcestershire, UK). Each measurement was performed at 25 °C with a fixed angle of 90° using a 640 nm wavelength.

2.4.9. Transmission electron microscope (TEM)

The morphology of the nanoparticles in water was analysed using TEM (JEM-2100F; JEOL, Tokyo, Japan). Each sample was prepared by absorbing nanoparticles-dissolved water in a 400-mesh copper grid (carbon-coated). The film on the grid was negatively stained by dropping a 1% phosphotungstic acid solution. An accelerated voltage of 200 kV was used to observe the grid.

2.5. Solubility test

An excess amount of each sample was added to 1 ml distilled water and vortexed for 5 min. The samples were then placed in a mechanical shaker in a water bath (Daihan Scientific, Wonju, South Korea) for 7 d to reach solubility equilibrium while maintaining the temperature at 25 °C and shaking at 100 rpm. After 7 d, the samples were centrifuged at 10,000 × *g* for 10 min. The supernatant was then filtered and analysed by HPLC.

2.6. Dissolution study

To compare the dissolution profiles of ESD and CSD, the paddle method (USP apparatus II) was employed. The evaluation was conducted in 900 ml distilled water, simulated gastric fluid (SGF without enzyme, pH 1.2) and simulated gastric intestinal fluid (SIF without enzyme, pH 6.8), with the rotation speed set at 100 rpm. Each sample was placed inside a dissolution tester (Vision® Classic 6; Hanson Research Co., Chatsworth, CA, USA) and the temperature of the dissolution medium was maintained at 37 ± 0.5 °C.

2.7. In vitro cytotoxicity and apoptosis assays

Human colon cancer cells (HCT-116) were sourced from the Korean Cell Line Bank (Seoul, South Korea), and culture with Dulbecco's modified Eagle's medium (DMEM) (HyClone Laboratories, Inc.). The media was supplemented with 10% Fetal bovine serum (FBS) (HyClone Laboratories, Inc.), 100 U/ml penicillin G sodium, and 100 μg/ml streptomycin sulfate at 37 °C in a humidified atmosphere (5% CO_2 and 95% air atmosphere). For cytotoxicity assessment, MTT assays were conducted. HCT-116 cells were seeded in a 96-well plate (3×10^4 per well) and incubated overnight. The cells were treated with nanoparticles at various concentrations for 48 h. The cells were washed twice with PBS and incubated with 100 μl MTT (1.25 mg/ml) for 4 h. Subsequently, dimethyl sulfoxide (100 μl) was added to each well and microplate reader was utilized to measure absorbance at 570 nm. For apoptosis analysis, fluorescence-activated cell sorting (FACS, Verse flow cytometer, BD Biosciences, San Jose, CA, USA) was utilized. All of the protocols were the same, except that the cells were stained with Annexin-V and PI for 24 h. For the Live/Dead cell assay, the nanoparticle-treated cells were subjected to staining with the LIVE/DEAD Viability/Cytotoxicity Kit (Invitrogen, Waltham, MA, USA) according to the manufacturer's instructions. The stained cells were analysed using K1-Fluo Confocal Laser Scanning Microscope (Nanoscope Systems, Daejeon, South Korea).

2.8. In vivo antitumor efficacy

The human colorectal carcinoma cell (HCT 116; ATCC, Manassas, VA, United States) tumor xenograft model was established by subcutaneously injecting 1×10^6 HCT116 cells/100 μl into the right flanks of six-week-old female BALB/c nude mice. When the tumor volume reached approximately 100 mm^3, the mice were randomly assigned to four groups (control, drug powder, CSDN and ESDN), with each group containing six mice. The control group received treatment with a 1% sodium carboxymethylcellulose aqueous solution. The drug powder and the two formulations were likewise dispersed in this 1% sodium carboxymethylcellulose solution. Subsequently, the mice were orally administered daily for 14 d at a dose of 10 mg/kg/d, respectively. Body weight and tumor volume were measured every other d. The tumor volume was measured as length × $width^2/2$, using digital Vernier caliper. All animal procedures were carried out in strict accordance with the recommendations of Yeungnam University's Guidelines for the Care and Use of Laboratory Animals and approved by Yeungnam University's Animal Ethics Committee.

2.9. Histopathological and immunohistochemical assessment

When the *in vivo* anticancer efficacy test was over, tumors and major organs (heart, liver, spleen, lung and kidney) were harvested for histopathological assessment. They were embedded in paraffin and sections (3–4 μm) were stained with hematoxylin and eosin (H&E) for microscopic imaging. In addition, tumor cell apoptosis (cleaved caspase-3 and PARP), angiogenesis (CD31) and cell proliferation (Ki-67) markers were examined under avidin-biotinperoxidase complex (ABC)-based immunohistochemistrical stain, using primary antisera.

2.10. Pharmacokinetic study

2.10.1. Animals

Male Sprague-Dawley rats were used for the *in vivo* study. The animals were obtained from Koatech (Pyeongtaek, South Korea) and weighed 300 ± 20 g. All of the animal procedures were approved by the Institutional Animal Care and Use Committee (IACUC) at Hanyang University. The standard procedures for animals, before, during, and after the *in vivo* study, were performed in accordance with the NIH policy.

2.10.2. Administration and blood collection

The pharmacokinetic study was performed based on the established method [21]. Briefly, the rats were divided into three groups, with six rats in each group. Drug powder and the two formulations were suspended in 1% sodium carboxymethylcellulose and orally administered to rats at a dose of 20 mg/kg. At a pre-determined time, 0.25 ml blood was collected through the inserted tube. The collected samples were centrifuged, and the supernatant (plasma) was separated.

2.10.3. Blood sample analysis

Each plasma sample (100 μl) was mixed with sorafenib solution (200 μl, 10 μg/ml prepared in acetonitrile) as the internal standard. The samples were then centrifuged and the supernatant was separated. The supernatant (50 μl) was analysed for regorafenib quantification by HPLC (Method 2 in supplementary materials).

2.11. Statistical analysis

Statistical significance ($P < 0.05$) was confirmed by Student's *t*-tests (comparing a pair of groups) and one-way ANOVA test followed by least-significant differences (comparing three or more groups). Statistical calculations were performed using SPSS® version 26 (IBM, Bethesda, MD, USA).

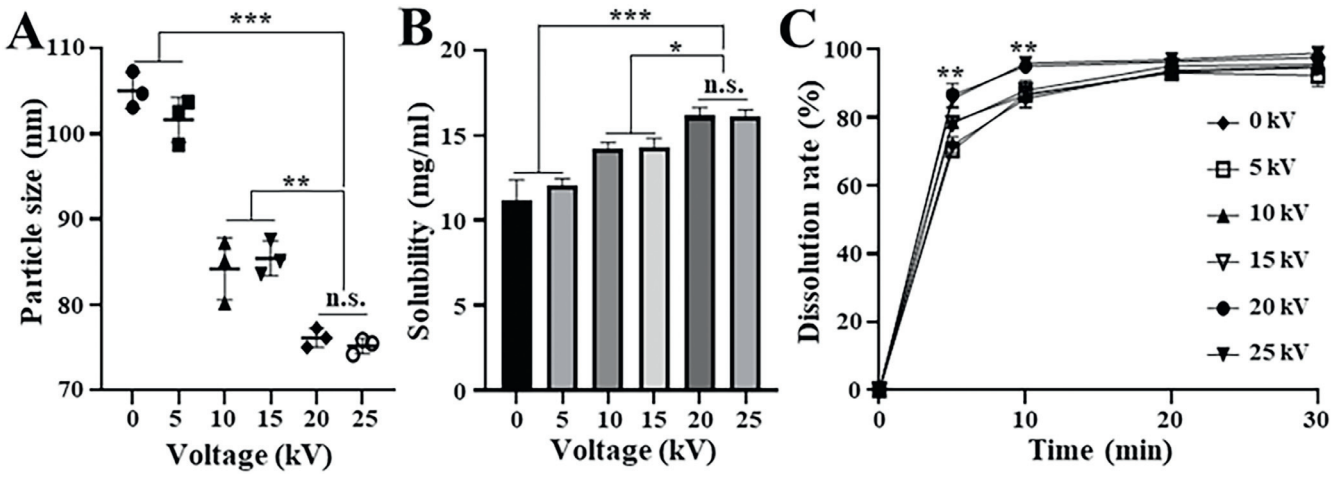

Fig. 1 – Effects of voltage on ESDN: (A) Particle size. (B) Solubility. (C) Dissolution rate (%) in water. Each value represents the mean ± SD ($n = 3$); *P < 0.05, **P < 0.01, ***P < 0.001; n.s. not significant).

3. Results and discussion

3.1. *Optimization of voltage in ESD*

Based on the carrier screening technique, copovidone and SDS were selected. Then, various ESDN were obtained by modulating the voltage. It was demonstrated that nanoparticle sizes decreased with increasing voltage (Fig. 1A). However, there were no significant differences observed when the voltage was increased from 20 to 25 kV. Similar trends were observed in solubility and dissolution results (Fig. 1B and 1C). Solubility improved in proportion to the voltage increment. Furthermore, rapid release and higher dissolution rates (%) were observed at voltage settings of 20 and 25 kV. Increasing the voltage from 20 to 25 kV hardly provided significant differences in solubility and dissolution profiles.

3.2. *Drying kinetic study and yield analysis*

Two types of nanoparticles, comprising the same components, were prepared by CSD and ESD (Table S2). When the drying time was consistent, there was a significant difference between the two techniques in terms of the outlet temperature at every time point (Fig. 2A and 2B). Moreover, both processes provided a yield (%) over 70%, showing no significant differences (Fig. 2C). In ESD, a low drying temperature was sufficient to evaporate the solvent, while a relatively high operating temperature was required for CSD (Fig. 2D). The conventional drying technique is composed of two phases: constant-rate drying and falling-rate drying. Generally, a high amount of thermal energy is required to evaporate the remaining solvent from the core of the particle due to the shell formation during the falling-rate drying period [22-24]. However, the drying process in the ESD is a single phase consisting of constant-rate drying. The electrostatic force drove the solvent to the outside, inducing solvent migration and solid materials to the inside of the droplet. This effect removed the need for the falling rate period by inhibiting shell formation on the outer side of the particle. Consequently, the thermal energy of the heated air effectively participated in the drying process without the need to raise the operating temperature.

3.3. *Powder morphology and size class distribution*

The powder morphologies of CSDN and ESDN were compared by SEM (Fig. 3A). The drug powder had an irregular and rectangular crystalline form (Fig. S1A). In contrast to the drug powder, sphere-shaped particles appeared in both systems with decreased size. When comparing CSDN and ESDN the latter presented smaller particles with better uniformity. The particle size reduction in ESD was much more noticeable when viewed at high magnification (×10 K).

The size class distribution was evaluated via the laser diffraction method. The ESDN (2.01 ± 0.08) showed a significantly higher uniformity index than CSDN (0.62 ± 0.09) (Fig. 3B). In addition, ESDN exhibited approximately 2 times larger specific surface area than CSDN (Fig. 3C). A significant reduction in particle size was shown in ESDN compared to CSDN, despite no substantial differences in surface morphology (Fig. S2). Consequently, the smaller particle size of ESDN led to a larger specific surface area than that of CSDN, as the specific surface area is proportional to the reduction in particle size [25]. ESDN showed decreased D10, D50 and D90 values, compared to the drug powder and CSDN (Fig. S1B and 3D). According to the D50 values, ESD generated particles approximately 42 % smaller in size than CSD. Therefore, these results indicated that ESD contributed to fabricating nanoparticles with smaller sizes with even distribution.

Both particle size reduction and morphology changes occurred during the manufacture of nanoparticles. Furthermore, the electrostatic force resulted in a significantly reduced particle size compared to CSD. In CSD, compressed hot air gas is the only force that atomizes the feed solution. However, in the ESD, electrostatic force (high voltage with low amperage charge) induced the solvent to have a large electric

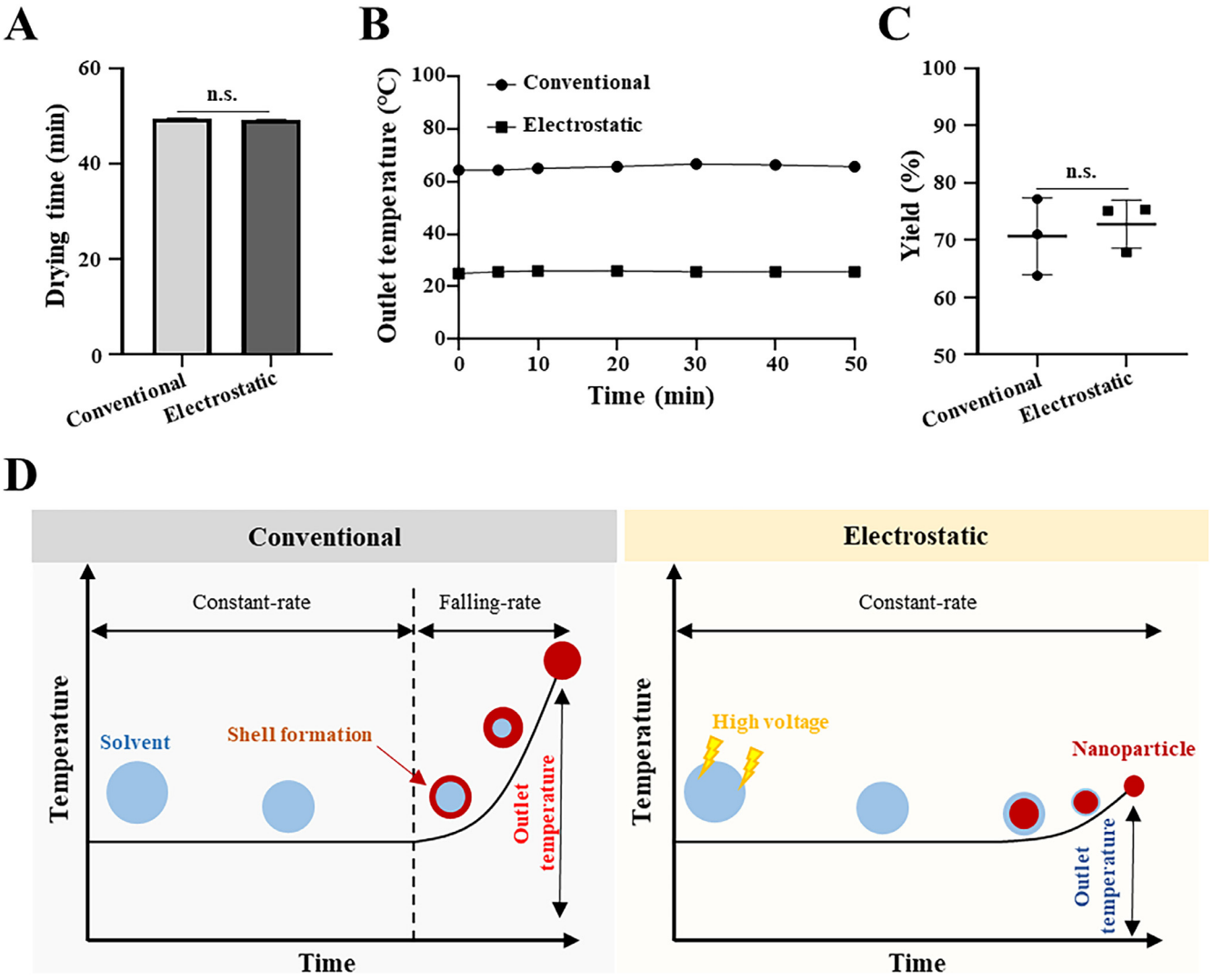

Fig. 2 – Drying kinetic study and yield analysis. (A), Drying time. (B) Drying kinetic profiles. (C) Yield analysis. (D) Schematic illustration of drying kinetic mechanisms. Each value represents the mean ± SD (n = 3), n.s. not significant.

dipole moment, since they were relatively polar compared to the drug and carriers. On the contrary, the drug was forced to have a small dipole moment owing to its less polar property. Subsequently, the solvent molecules repel each other and move to the outer part of the droplet, while the drug and hydrophilic carriers remain at the centre. As a result, compact ultrafine nanoparticles were produced via ESD. Conversely, there was no additional force that brought the drug and carriers to the core during CSD. Therefore, relatively large particles were produced in conventional method.

3.4. *Physicochemical characterization*

The thermal aspects of the drug powder, physical mixtures, and the nanoparticles were examined by DSC (Fig. 4A). The drug powder presented a distinguishing peak at approximately 206 °C, corresponding to its melting point and indicating its crystalline form (Fig. 4Aa). The DSC curve of the physical mixtures exhibited the same endothermic peak as regorafenib at 206 °C, indicating that the excipients (copovidone and SDS) scarcely affected the thermal properties of the drug (Fig. 4Ab). Compared to the drug powder, the endothermic peak of the physical mixtures showed reduced intensity, since the amount of regorafenib was relatively less than that of the pure drug powder. However, no apparent peak was detected in either of the nanoparticles (Fig. 4Ac and 4Ad). The results demonstrated that the thermal characteristics of the drug were influenced by both conventional and electrostatic-spray-drying. The crystallinity of the prepared samples was confirmed by XRD (Fig. 4B). Various peaks were observed over the angles of the drug powder, indicating their crystalline nature (Fig. 4Ba). The unique XRD patterns of the drug are shown in the physical mixtures (Fig. 4Bb). In contrast, the patterns disappeared over all angles in both nanoparticles (Fig. 4Bc and 4Bd). Accordingly, the crystalline nature of the drug was influenced during the conventional and ESD processes. Based on the DSC and XRD results, the drug powder was present in a crystalline state. However, the

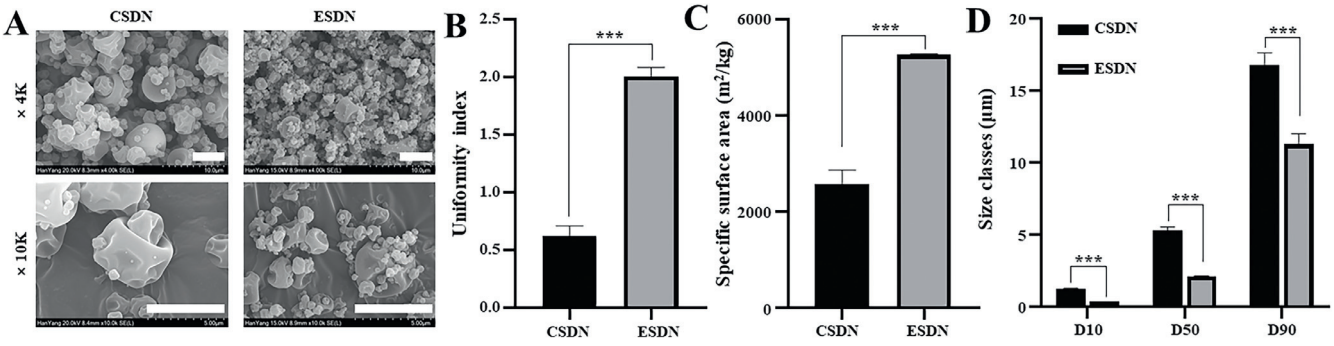

Fig. 3 – Morphology and particle size distribution analysis. (A) SEM images (Scale bar = 5 μm). (B) Uniformitiy idex (C). Specific surface area. (D) Size classes distribution. Each value represents the mean ± SD (n = 3), ***$P < 0.001$.

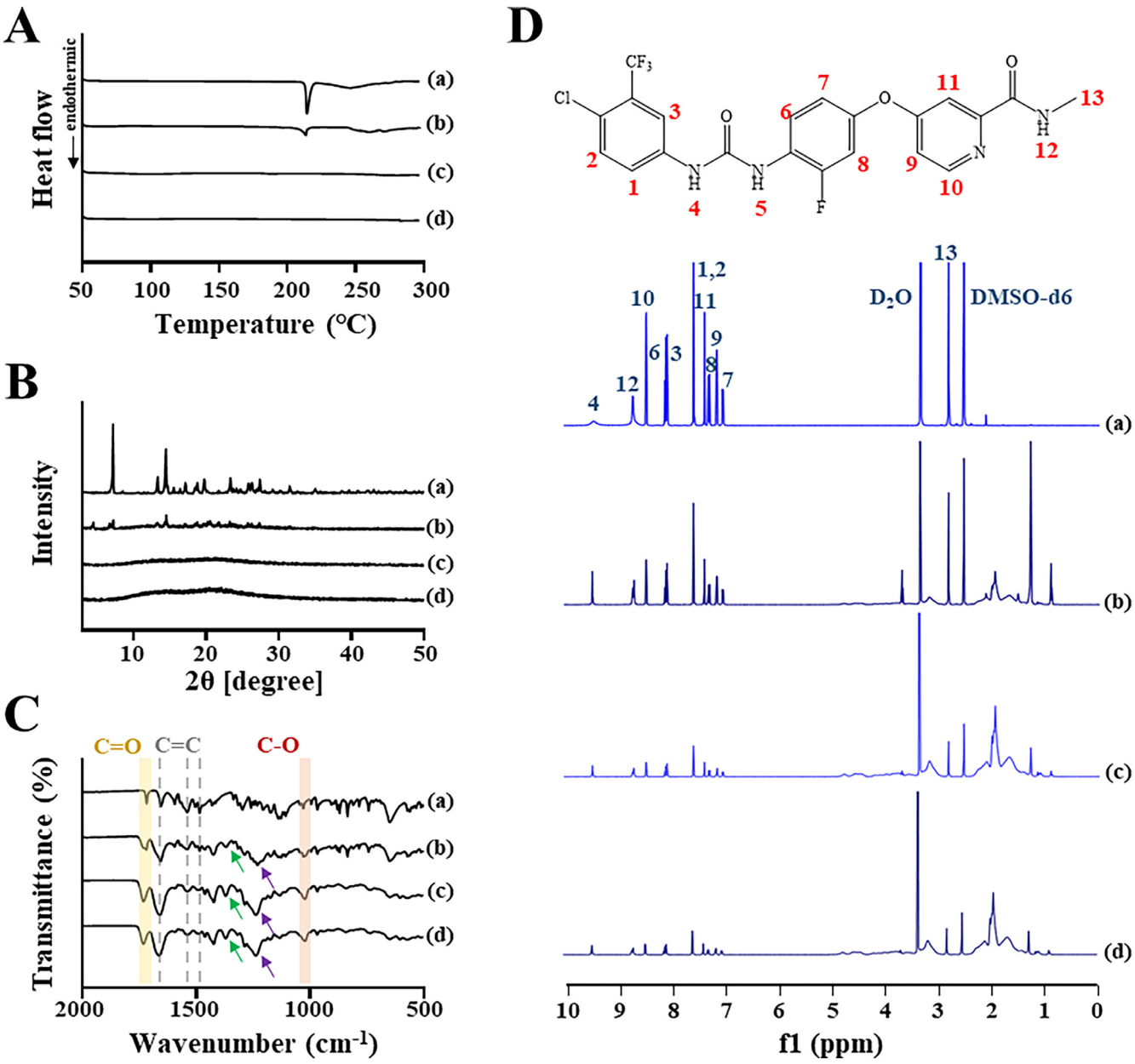

Fig. 4 – Physicochemical characterization: (A) DSC analysis, (B) XRD patterns, (C) FTIR spectra, and (D) ^{1}H NMR spectra of (a) drug powder (b) physical mixtures of drug, copovidone and SDS; (c) CSDN and (d) ESDN.

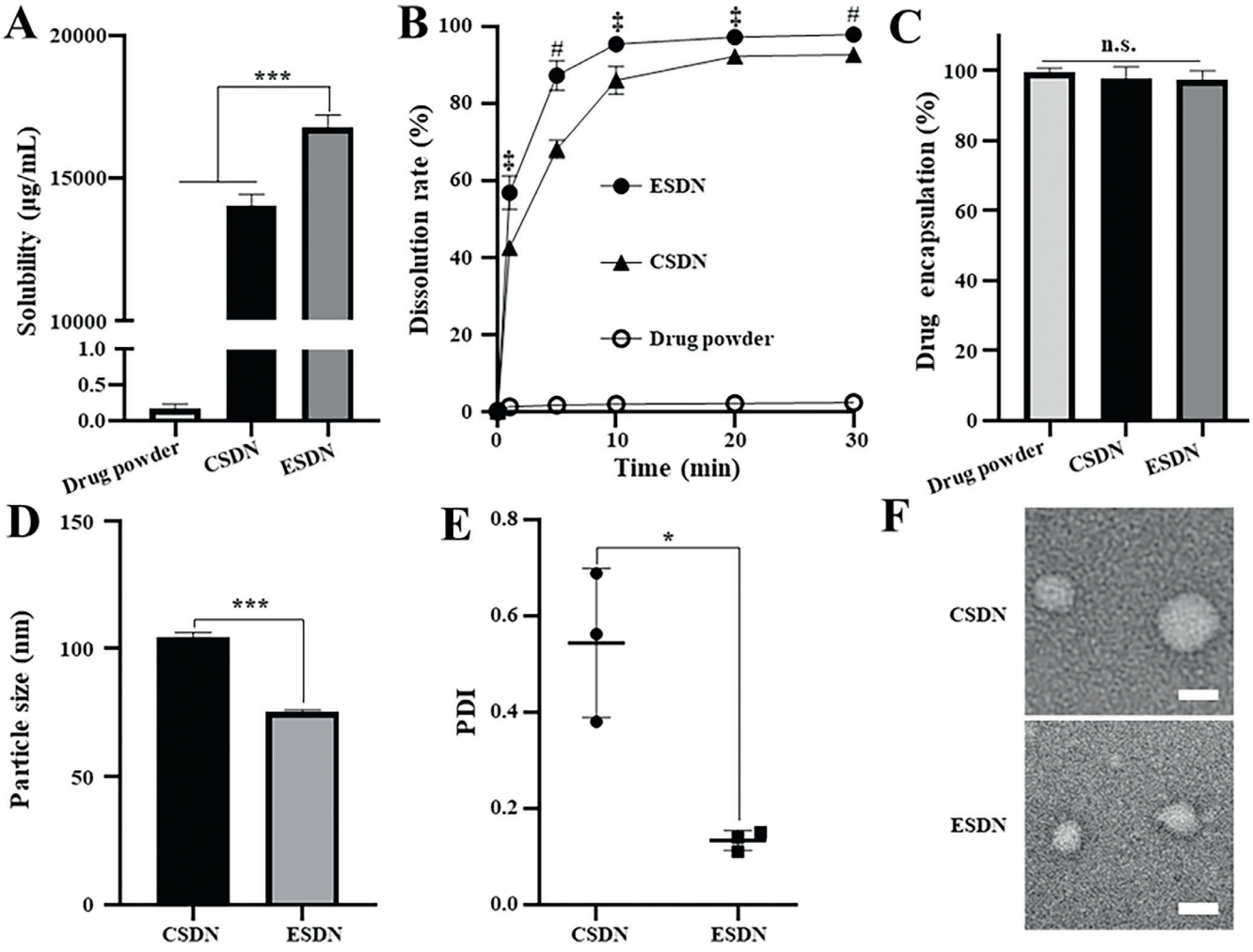

Fig. 5 – Functional properties in water: (A) Solubility. ***$P < 0.001$. (B) Dissolution rate (%) in water. $^{‡}P < 0.01$, $^{\#}P < 0.001$ compared to CSDN. (C) Encapsulation efficiency (%). n.s. not significant. (D) Particle size ***$P < 0.001$. (E) PDI. *$P < 0.05$. (F) TEM images (Scale bar = 100 nm). Each value represents the mean ± SD ($n = 3$).

crystalline state of the drug transformed into an amorphous state in both nanoparticles.

The alterations of molecular state of the drug in both systems were evaluated by FT-IR analysis (Fig. 4C). Generally, the occurrence of molecular interactions influences the rigidity of the drug. Several studies have shown that altered flexibility in molecular structure prevented the drug from permeating the gastrointestinal membrane, reducing oral bioavailability [21,26]. It is widely reported that spray drying process scarcely induces molecular interactions between the drug and excipients [27]. However, no studies have elucidated the possibility that high electrostatic force might induce molecular interactions. Therefore, it was important to investigate whether high electrostatic forces during the ESD provoke molecular interaction between the drug and carriers. In FTIR spectra, the drug powder presented characteristic stretches at 1720 cm^{-1} and 1040 cm^{-1} indicating carbonyl groups (C=O) and phenyl ether groups (C–O), respectively (Fig. 4C-a). Moreover, peaks corresponding to aromatic ring (C=C) stretch bands were observed at 1650 cm^{-1}, 1550 cm^{-1} and 1490 cm^{-1} in the drug powder. The specific signals were observed in physical mixtures, suggesting there were no molecular interaction between the drug and carriers (Fig. 4Cb). Similarly, CSDN and ESDN provided all the distinguishing peaks shown in the drug powder, expecting high electrostatic force hardly induced the creation of complex formation or hydrogen bonding (Fig. 4Cc and 4Cd). At the same time, it was elucidated that the drug was successfully encapsulated in the nanoparticles. However, the unique peaks of the drug are shown to be weakened in CSDN and ESDN, as they are diluted by the strong intensity of other peaks from the excipients comprising the nanoparticles. Particularly, the distinctive peaks of copovidone and SDS were observed around 1280 cm^{-1} and 1400 cm^{-1}, respectively, in CSDN and ESDN [28,29]. Along with the FT-IR results, chemical shift values in ^{1}H NMR spectra were evaluated to detect the changes of molecular stated in the drug (Fig. 4D). ^{1}H NMR spectra of regorafenib and its assigned atom numbers are shown in Fig. 4 Da. The chemical shifts of the drug were not observed in physical mixtures, assuming molecular interaction hardly occurred when the drug and carriers were simply blended (Fig. 4Db). Furthermore, there were no significant differences

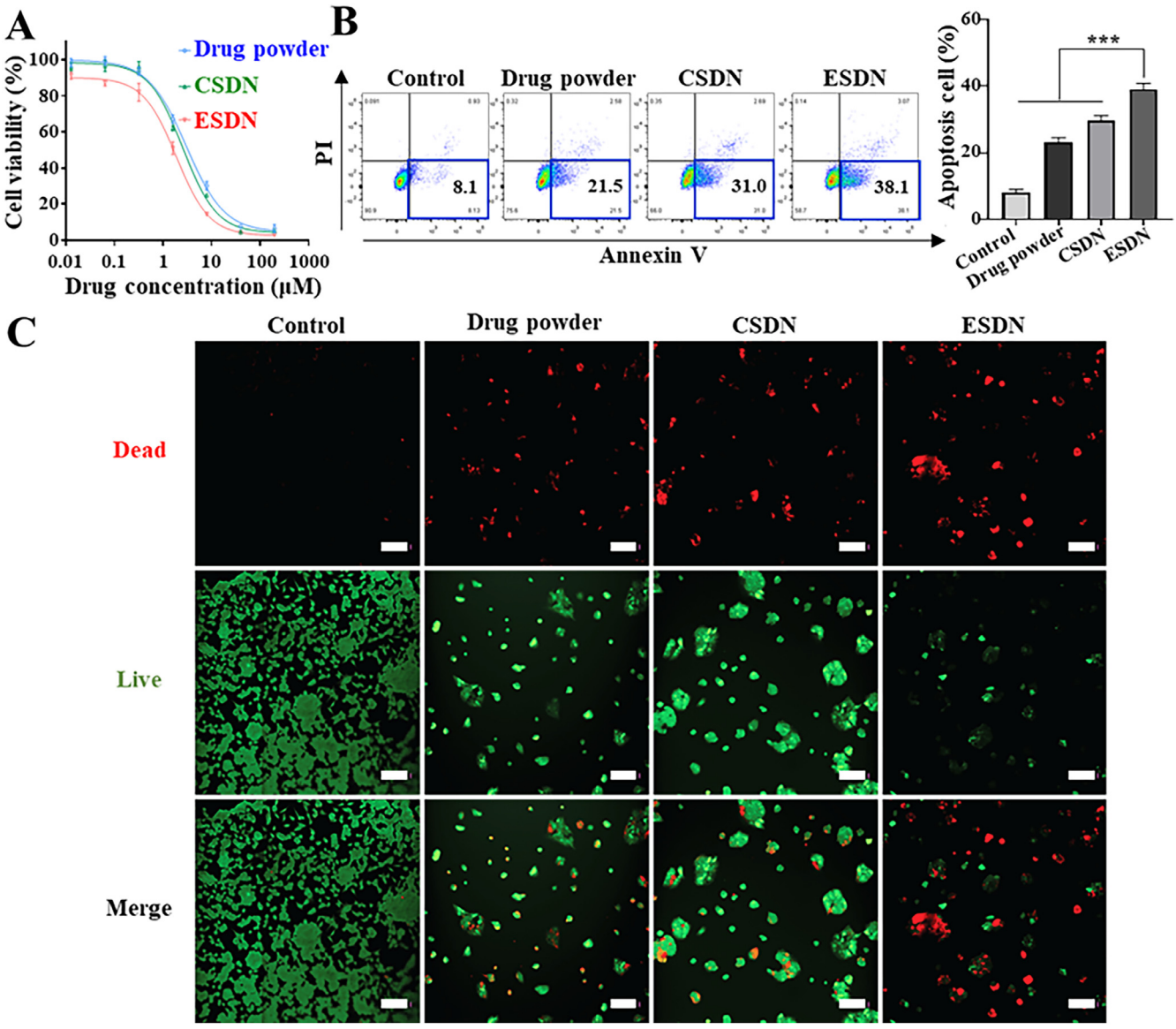

Fig. 6 – *In vitro* cytotoxicity assays: (A) Concentration-dependent cytotoxicity profiles. (B) FACS analysis. (C) Confocal images of live/dead assay. (*$P < 0.001$).**

between the drug powder, CSDN and ESDN, suggesting that electrostatic force barely induced molecular interactions (Fig. 4Dc and 4Dd). Furthermore, the distinguishing peaks of the drug, observed in both nanoparticles, confirmed that the drug was loaded in both nanoparticles. Therefore, electrostatic energy in the ESD hardly affects the molecular state of the drug, compared to CSD.

3.5. *Solubility and dissolution profile*

The comparative drug solubility and dissolution profiles are shown in Fig. 5A and 5B, respectively. The drug powder had an aqueous solubility of 0.16 ± 0.10 μg/ml, indicating poor water solubility. Both nanoparticles significantly enhanced drug solubility compared to that of the drug powder. In particular, ESDN (16,148.75 ± 451.67 μg/ml) presented significantly higher solubility than CSDN (14,882.40 ± 389.35 μg/ml). Moreover, both nanoparticles exhibited a significantly increased dissolution rate (%) compared to drug powder during the entire study period ($P < 0.001$). The ESDN showed rapid release with significantly enhanced dissolution rate compared to CSDN. The trends in the dissolution test results remained consistent whether conducted in SGF or SIF. However, the dissolution rate values for drug powder, CSDN, and ESDN were significantly lower in SGF as the dissolution medium compared to when water or SIF was used. There were no significant differences among the drug powder, CSDN and ESDN in terms of drug encapsulation efficacy (Fig. 5C). During the fabrication of nanoparticles, the decomposition of the drug could lead to reduced encapsulation efficiency. However, the encapsulation efficiency of ESDN, which showed no significant difference from that of free drug

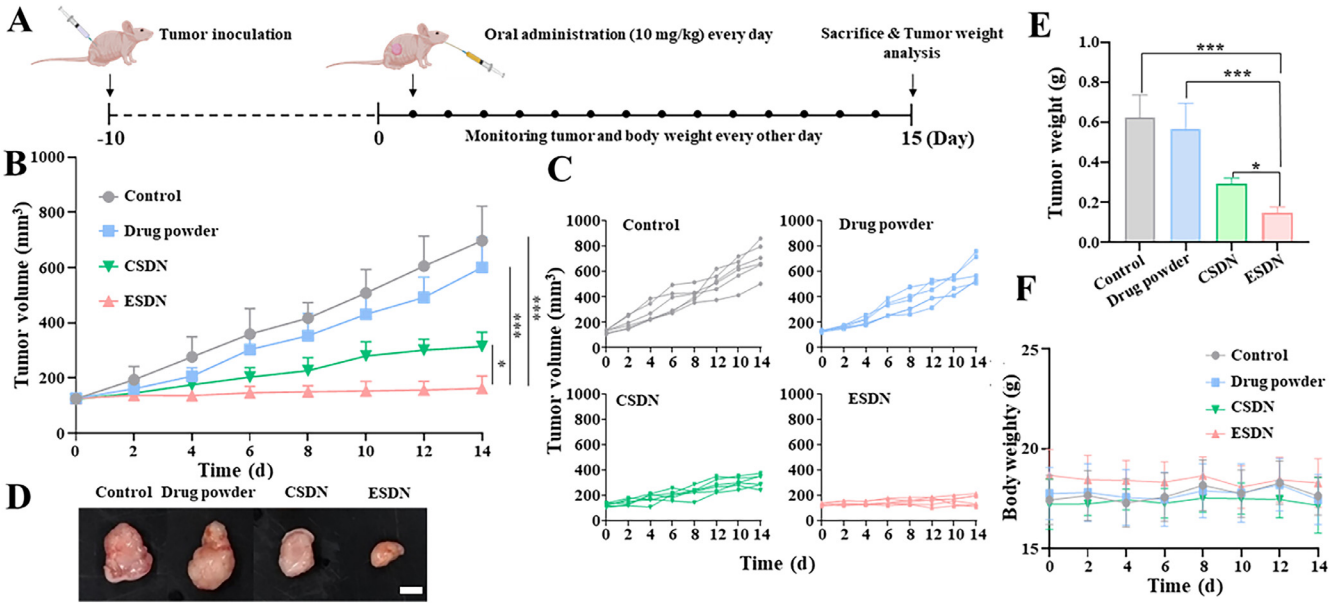

Fig. 7 – *In vivo* antitumor efficacy: (A) Schematic illustration of tumor inoculation and dosing schedules. (B and C) Tumor growth curves; (D), Dissected tumor images at Day 15. Scale bar = 0.5 cm; (E), Dissected tumor weight at Day 15; (F), Body weight of tumor-bearing mice during the *in vivo* study. *P < 0.05, ***P < 0.001.

powder, demonstrated that neither electrostatic forces nor temperature substantially induced the denaturation of the drug.

After the dissolution test in water, the particle sizes and PDI of both nanoparticles in water were assessed. The particle size and PDI value of ESDN was significantly smaller than that of CSDN (particle size; 75.2 ± 0.8 nm *vs.* 104.7 ± 1.6 nm, PDI; 0.133 ± 0.020 vs. 0.543 ± 0.155) (Fig. 5D and 5E). The size distribution chart further elucidated the superior uniformity of particle size in ESDN compared to CSDN. (Fig. S4). The morphology of the nanoparticles in water was observed using TEM (Fig. 5F). It was confirmed that when both formulations were dissolved in water, the drug was dispersed as nanoscale spheres; however, ESDN exhibited significantly decreased particle size with superior homogeneity compared to CSDN.

One of the main reasons for the increased solubility in nanoparticles, compared to the drug powder, is amorphous state. Based on the DSC and XRD results, the hydrophobic crystalline state of the drug transformed into a hydrophilic amorphous state in both formulations. In amorphous solids, the molecules are randomly oriented with a lack of lattice energy compared to crystalline solids. Consequently, when ESDN were dissolved in water, supersaturation of the drug with high chemical potential energy occurred, leading to higher drug solubility than the drug powder. When comparing ESDN and CSDN, particle size distribution results explained the differences in solubility and dissolution profiles. In ESD, nanoparticles with minimized size and increased specific surface area were produced, as compared to the conventional process, owing to the application of electrostatic force. Hence, ESDN had a larger contact area with water than CSDN when dissolved in water. As a result, ESDN were exposed to a more hydrophilic microenvironment than CSDN. Thereby, ESDN exhibited significantly higher solubility with rapid drug release (%), compared to CSDN.

3.6. *In vitro cytotoxicity profiles*

The drug powder, CSDN and ESDN were suspended in 0.1% DMSO and treated to HCT-116 cells due to poor solubility of regorafenib. After 48 h of incubation, MTT assay was conducted to evaluate the cytotoxicity of the nanoparticles. The corresponding concentration-dependent cytotoxicity profiles are exhibited in Fig. 6A. The ESDN showed significantly higher cytotoxicity than both drug powder and CSDN. The IC50 value for ESDN (1.89×10^{-6} M) was significantly decreased from the drug powder (3.02×10^{-6} M) and CSDN (2.57×10^{-6} M), indicating their enhanced cytotoxicity in HCT-116 cells. According to the FACS results in Fig. 6B, early apoptosis occurred in HCT-116 cells after treating drug powder, CSDN and ESDN. In particular, ESDN (39.0% ± 1.9%) induced the highest rate of early apoptosis in HCT-116 cells, followed by CSDN and drug powder. The confocal images further revealed the enhanced cytotoxicity of ESDN in HCT-116 cells (Fig. 6C). The *in vitro* cytotoxicity studies demonstrated that the solubility of the drug powder and the nanoparticles influenced their cytotoxic effects. Typically, cells struggle to uptake small-molecule drugs such as regorafenib unless they are fully dissolved in the cell media. Even if the free drug powder was dissolved in the media and internalized by the cells, it was expected to be metabolized and cleared more rapidly than drug-loaded nanoparticles, resulting in lower efficacy. Consequently, ESDN with enhanced solubility exhibited greater cytotoxicity in HCT-116 cells compared to those with lower solubility.

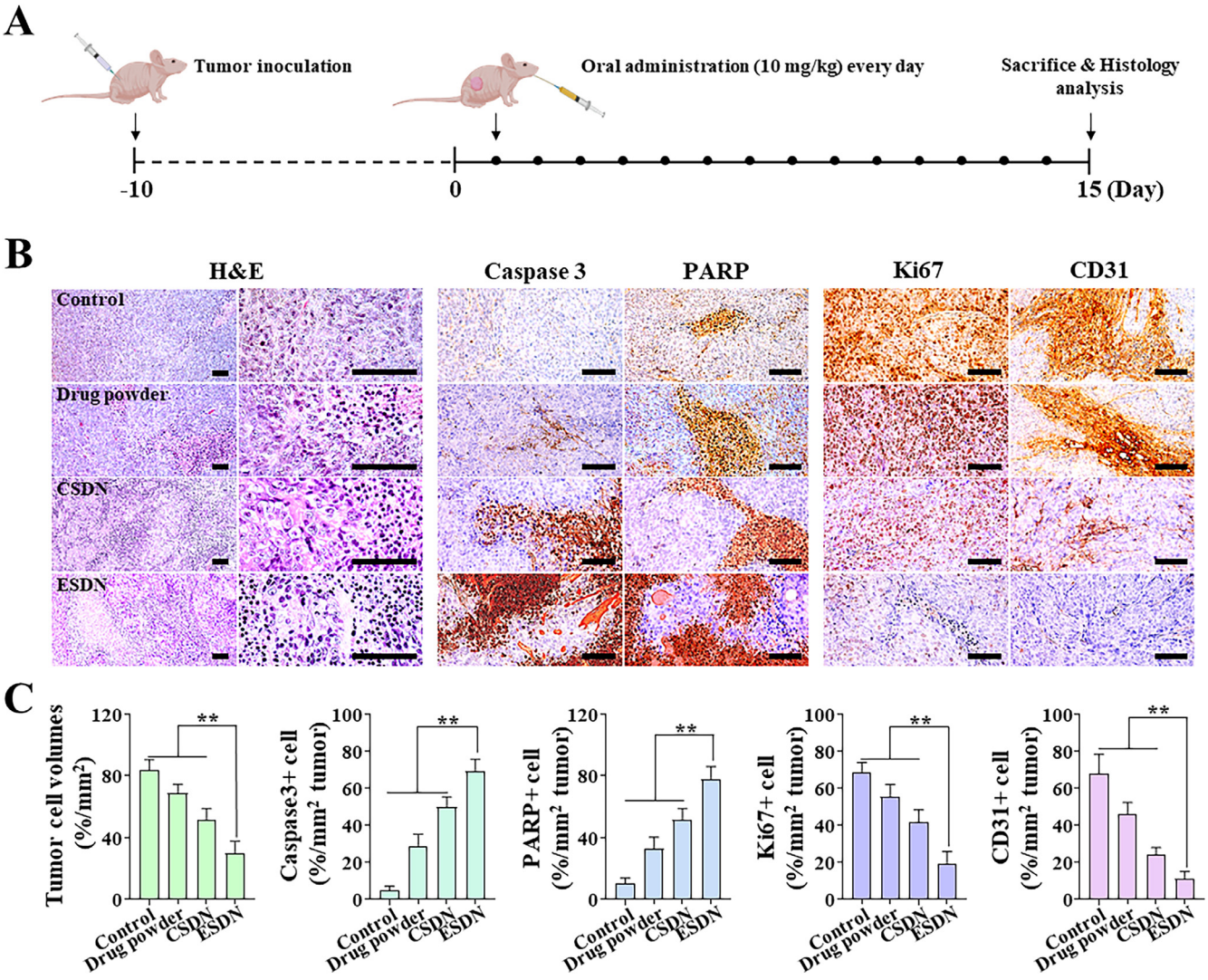

Fig. 8 – Histology evaluation: (A) Scheme of histology analysis design. (B and C), H&E staining and expression levels of caspase-3, PARP, CD31 and Ki67 in tumors. Scale bar = 120 μm; **$P < 0.01$).

3.7. *In vivo antitumor efficacy*

We further performed the *in vivo* antitumor efficacy experiment in mice (Fig. 7). The study scheme is illustrated in Fig. 7A. The tumor volume of ESDN-treated groups was significantly smaller than those of the control, drug powder and CSDN-treated groups (Fig. 7B and 7C). The tumor inhibition efficacy increased in the following order: control < drug powder < CSDN < ESDN. According to the dissected tumor analysis, ESDN remarkably inhibited tumor growth compared to the control, drug powder and CSDN (Fig. 7D and 7E). There were no significant variations in terms of body weight in all groups of mice (Fig. 7F).

At Day 15, histology analysis was carried out for the dissected tumors (Fig. 8). The H&E staining revealed that noticeable decreases of tumor cell volumes were observed in ESDN-treated groups, as compared to those of control, drug powder and CSDN-treated groups. Furthermore, ESDN significantly increased the expression of apoptosis markers (caspase-3 and PARP), compared to control, drug powder and CSDN (control < drug powder < CSDN < ESDN). In contrast, the proliferation (Ki-67) and angiogenesis (CD31) markers were the highest in the control and ESDN-treated groups showed the lowest expression rate.

Moreover, *in vivo* toxicity study was conducted to determine whether the remarkable antitumor efficacy of ESDN could result in toxicity in other organs. Compared to the control group, which was treated only with a 1 % sodium carboxymethylcellulose aqueous solution, the ESDN-treated group exhibited negligible pathological findings in the liver and other vital organs (Fig. S5). The results revealed that ESDN showed noticeable efficacy in treating tumors with minimal toxicity.

3.8. *Pharmacokinetic study in rats*

The oral bioavailability of regorafenib in drug powder, CSDN and ESDN was compared in rats. Fig. 9 presents the plasma concentration *versus* time profiles of regorafenib after oral administration. The plasma concentrations of ESDN were

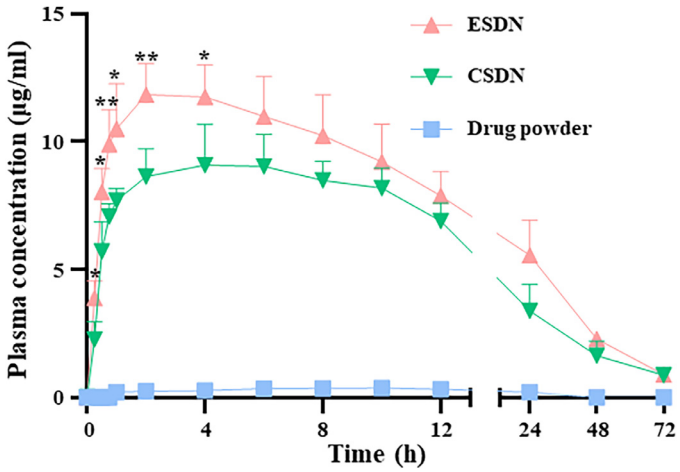

Fig. 9 – Plasma concentration–time profiles of regorafenib. Each value represents the mean ± SD ($n = 6$). *$P < 0.05$ and **$P < 0.01$ compared to CSDN.

Table 1 – Pharmacokinetic parameters. Each value represents the mean ± SD ($n = 6$). **$P < 0.01$ compared to drug powder and CSDN, #$P < 0.05$ compared to drug powder.

	Drug powder	CSDN	ESDN
AUC (μg·h/ml)	6.79 ± 1.28	249.78 ± 40.36	334.75 ± 34.10**
C_{max} (μg/ml)	0.37 ± 0.11	9.08 ± 1.18	11.83 ± 1.20**
T_{max} (h)	8.00 ± 2.00	5.50 ± 1.91	3.50 ± 1.91#
K_{el} (h^{-1})	0.039 ± 0.009	0.030 ± 0.002	0.032 ± 0.001
$T_{1/2}$ (h)	17.70 ± 4.55	23.54 ± 1.89	21.73 ± 0.60

significantly higher than those of the drug powder over the entire study period ($P < 0.001$). In addition, the plasma concentration of ESDN was significantly higher than that of CSDN in the initial period (0.25, 0.5, 0.75, 1, 2 and 4 h). Pharmacokinetic parameters were calculated according to the above plasma concentration–time profiles (Table 1). Compared to the drug powder (6.79 ± 1.28 μg·h/ml), ESDN (334.75 ± 34.10 μg·h/ml) significantly enhanced the AUC values by 49.3 times, ($P < 0.001$). Specifically, ESDN significantly improved oral bioavailability compared to CSDN $P < 0.01$). Similarly, the C_{max} value of ESDN (11.83 ± 1.20 μg/ml) was significantly higher than that of the drug powder (0.37 ± 0.11 μg/ml, $P < 0.001$) and CSDN (9.08 ± 1.18 μg/ml, $P < 0.01$). There were no significant differences in the K_{el} and $t_{1/2}$ values between the drug powder and the two nanoparticles ($P > 0.05$). Unlike CSDN (5.50 ± 1.91 h), the T_{max} of ESDN (3.50 ± 1.91 h) was significantly faster than that of the drug powder (8.00 ± 2.00 h, $P < 0.05$). The results of the pharmacokinetic study were consistent with the solubility, dissolution and cytotoxicity profiles. The poor solubility of the drug powder results in inadequate absorption. However, ESDN are expected to supersaturate in gastric acid owing to their enhanced aqueous solubility. Moreover, ESDN showed greater enhancements in solubility, accelerated release, and heightened dissolution rates compared to CSDN, owing to their substantially reduced particle size and improved uniformity. Consequently, ESDN had a higher plasma concentration during the entire period of the pharmacokinetic study, resulting in improved oral bioavailability and increased C_{max}, with rapid therapeutic onset compared to CSDN.

Upon integrating the results from pharmacokinetic studies and *in vivo* antitumor assays, we confirmed that the enhanced anticancer efficacy of ESDN can be attributed to its increased oral bioavailability. Additionally, we determined that the fine particle size of ESDN, characterized by increased uniformity and specific surface area, along with improved solubility, contributed to the enhancement of its oral bioavailability.

4. Conclusion

In conclusion, this study suggested ESD as an advanced preparation method for improving oral bioavailability of poorly water-soluble drugs, effectively addressing the limitations associated with CSD methods. The ESD produced fine and homogenous nanoparticles, which showed significantly decreased particle size compared to CSDN. In particular, mild temperature was sufficient to induce solvent evaporation and facilitate nanoparticle fabrication through ESD. The ESDN presented significantly improved solubility, dissolution rate (%), *in vitro* cytotoxicity, oral bioavailability and *in vivo* antitumor efficacy compared to drug powder and CSDN. Herein, the compositions of ESDN and CSDN were identical; however, ESDN showed superior efficacy due to their uniform size distribution and small particle size with a large specific surface area through ESD. To conclusively establish the superiority of ESDN, a comparative pharmacokinetic study with the commercial product of regorafenib is essential. Given that the commercial product of regorafenib is administered as a tablet, future pharmacokinetic studies should be conducted in beagle dogs or human subjects. Although this study used regorafenib as a model drug, the advantages of ESD are expected to be more definitively confirmed in future studies using heat-sensitive model drugs.

Conflicts of interest

The authors report no conflicts of interest in this work.

CRediT authorship contribution statement

Jung Suk Kim: Writing – original draft, Funding acquisition, Formal analysis, Data curation, Conceptualization. **Seunghyun Cheon:** Writing – original draft, Methodology, Investigation, Formal analysis, Data curation, Conceptualization. **Mi Ran Woo:** Methodology. **Sanghyun Woo:** Methodology. **Jee-Eun Chung:** Supervision. **Yu Seok Youn:** Supervision. **Kyung Taek Oh:** Supervision. **Soo-Jeong Lim:** Supervision. **Sae Kwang Ku:** Supervision. **Bao Loc Nguyen:** Investigation. **Jong Oh Kim:** Writing – original draft, Methodology, Investigation, Formal analysis, Data curation, Conceptualization. **Sung Giu Jin:** Writing – original draft, Funding acquisition, Formal analysis, Data curation, Conceptualization. **Han-Gon Choi:** Writing – review & editing, Writing – original draft, Funding acquisition, Formal analysis, Data curation, Conceptualization.

Acknowledgements

This work was supported by the National Research Foundation of South Korea (NRF) grants funded by the South Korean government (MEST) (No. 2022R1A2C2004197, RS-2024-00407053 and RS-2023-00208448).

Supplementary materials

Supplementary material associated with this article can be found, in the online version, at doi:10.1016/j.ajps.2024.100953.

References

[1] Etter EL, Mei KC, Nguyen J. Delivering more for less: nanosized, minimal-carrier and pharmacoactive drug delivery systems. Adv Drug Deliv Rev 2021;179:113994.
[2] Poudel K, Park S, Hwang J, Ku SK, Yong CS, Kim JO, et al. Photothermally modulatable and structurally disintegratable sub-8-nm Au(1)Ag(9) embedded nanoblocks for combination cancer therapy produced by plug-in assembly. ACS Nano 2020;14:11040–54.
[3] Shen MY, Liu TI, Yu TW, Kv R, Chiang WH, Tsai YC, et al. Hierarchically targetable polysaccharide-coated solid lipid nanoparticles as an oral chemo/thermotherapy delivery system for local treatment of colon cancer. Biomaterials 2019;197:86–100.
[4] Fu SW, Li GT, Zang WL, Zhou XY, Shi KX, Zhai YL. Pure drug nano-assemblies: a facile carrier-free nanoplatform for efficient cancer therapy. Acta Pharm Sin B 2022;12:92–106.
[5] Wang YM, Ke J, Guo XM, Gou KJ, Sang ZT, Wang YB, et al. Chiral mesoporous silica nano-screws as an efficient biomimetic oral drug delivery platform through multiple topological mechanisms. Acta Pharm Sin B 2022;12:1432–46.
[6] Shetty K, Bhandari A, Yadav KS. Nanoparticles incorporated in nanofibers using electrospinning: a novel nano-in-nano delivery system. J Control Release 2022;350:421–34.
[7] Xia X, Yang X, Huang W, Xia X, Yan D. Self-assembled nanomicelles of affibody-drug conjugate with excellent therapeutic property to cure ovary and breast cancers. Nanomicro Lett 2021;14:33.
[8] Sahu BP, Baishya R, Hatiboruah JL, Laloo D, Biswas N. A comprehensive review on different approaches for tumor targeting using nanocarriers and recent developments with special focus on multifunctional approaches. J Pharm Investig 2022;52:539–85.
[9] Nespi M, Kuhn R, Yen CW, Lubach JW, Leung D. Optimization of spray-drying parameters for formulation development at preclinical scale. AAPS PharmSciTech 2022;23:28.
[10] Emami F, Shokooh MK, Yazdi SJM. Recent progress in drying technologies for improving the stability and delivery efficiency of biopharmaceuticals. J Pharm Investig 2023;53:35–57.
[11] Poozesh S, Bilgili E. Scale-up of pharmaceutical spray drying using scale-up rules: a review. Int J Pharm 2019;562:271–92.
[12] Szabo E, Zahonyi P, Brecska D, Galata DL, Meszaros LA, Madarasz L, et al. Comparison of amorphous solid dispersions of spironolactone prepared by spray drying and electrospinning: the influence of the preparation method on the dissolution properties. Mol Pharm 2021;18:317–27.
[13] Xue J, Wu T, Dai Y, Xia Y. Electrospinning and electrospun nanofibers: methods, materials, and applications. Chem Rev 2019;119:5298–415.
[14] Tanhaei A, Mohammadi M, Hamishehkar H, Hamblin MR. Electrospraying as a novel method of particle engineering for drug delivery vehicles. J Control Release 2021;330:851–65.
[15] Partheniadis I, Nikolakakis I, Laidmae I, Heinamaki J. A mini-review: needleless electrospinning of nanofibers for pharmaceutical and biomedical applications. Processes 2020;8:673.
[16] Mayrhofer L, Moras G, Mulakaluri N, Rajagopalan S, Stevens PA, Moseler M. Fluorine-terminated diamond surfaces as dense dipole lattices: the electrostatic origin of polar hydrophobicity. J Am Chem Soc 2016;138:4018–28.
[17] Demols A, Borbath I, Van den Eynde M, Houbiers G, Peeters M, Marechal R, et al. Regorafenib after failure of gemcitabine and platinum-based chemotherapy for locally advanced/metastatic biliary tumors: REACHIN, a randomized, double-blind, phase II trial. Ann Oncol 2020;31:1169–77.
[18] Akin Telli T, Bregni G, Vanhooren M, Saude Conde R, Hendlisz A, Sclafani F. Regorafenib in combination with immune checkpoint inhibitors for mismatch repair proficient (pMMR)/microsatellite stable (MSS) colorectal cancer. Cancer Treat Rev 2022;110:102460.
[19] Choi JE, Kim JS, Choi MJ, Baek K, Woo MR, Kim JO, et al. Effects of different physicochemical characteristics and supersaturation principle of solidified SNEDDS and surface-modified microspheres on the bioavailability of carvedilol. Int J Pharm 2021;597:120377.
[20] Kim JS, Din FU, Cho HJ, Choi YJ, Woo MR, Cheon SH, et al. Impact of carrier hydrophilicity on solid self nano-emulsifying drug delivery system and self nano-emulsifying granule system. Int J Pharm 2023;648:123578.
[21] Kim JS, Choi YJ, Woo MR, Cheon S, Ji SH, Im D, et al. New potential application of hydroxypropyl-beta-cyclodextrin in solid self-nanoemulsifying drug delivery system and solid dispersion. Carbohydr Polym 2021;271:118433.
[22] Boel E, Koekoekx E, Dedroog S, Babkin I, Vetrano MR, Clasen C, et al. Unraveling particle formation: from single droplet drying to spray drying and electrospraying. Pharmaceutics 2020;12:625.
[23] Mezhericher M, Levy A, Borde I. Modelling the morphological evolution of nanosuspension droplet in constant-rate drying stage. Chem Eng Sci 2011;66 884–69.

[24] Mezhericher M, Levy A, Borde I. Spray drying modelling based on advanced droplet drying kinetics. Chem Eng Proces Process Intensif 2010;49:1205–13.
[25] Xu J, Song M, Fang Z, Zheng L, Huang X, Liu K. Applications and challenges of ultra-small particle size nanoparticles in tumor therapy. J Control Release 2023;353:699–712.
[26] Veber DF, Johnson SR, Cheng HY, Smith BR, Ward KW, Kopple KD. Molecular properties that influence the oral bioavailability of drug candidates. J Med Chem 2002;45:2615–23.
[27] Lan Y, Xu M, Ohm JB, Chen B, Rao J. Solid dispersion-based spray-drying improves solubility and mitigates beany flavour of pea protein isolate. Food Chem 2019;278:665–73.
[28] Allahbakhsh A, Mazinani S. Influences of sodium dodecyl sulfate on vulcanization kinetics and mechanical performance of EPDM/graphene oxide nanocomposites. RSC Adv 2015;5:46694–704.
[29] Hu X, Sun M, Li Y, Tang G. Evaluation of molecular chaperone drug function: regorafenib and β-cyclodextrins. Colloids Surf B Biointerfaces 2017;153:61–8.